Relative roles of dynamic and thermodynamic processes in causing positive and negative global mean SST trends during the past 100 years

Zhibo Li[1], Tim Li[1,2], and Ying Sun[3]

[1]Key Laboratory of Meteorological Disaster, Ministry of Education (KLME) / Joint International Research Laboratory of Climate and Environmental Change (ILCEC) / Collaborative Innovation Center on Forecast and Evaluation of Meteorological Disasters (CIC-FEMD), Nanjing University of Information Science and Technology, Nanjing, China

[2]International Pacific Research Center and Department of Atmospheric Sciences, School of Ocean and Earth Science and Technology, University of Hawaii, Honolulu, Hawaii, USA

[3]National Climate Center, Laboratory for Climate Studies, China Meteorological Administration, Beijing, China

Submitted to ***Dynamics of Atmospheres and Oceans***

Corresponding author: Tim Li, Department of Atmospheric Sciences, School of Ocean and Earth Science and Technology, University of Hawaii, Honolulu, Hawaii, USA.
Email: timli@hawaii.edu

Abstract

Global mean surface temperature (GMST) during 1910 - 2012 experienced four alternated rapid warming and warming hiatus phases. Such a temporal variation is primarily determined by global mean sea surface temperature (SST) component. The relative roles of ocean dynamic and thermodynamic processes in causing such global mean SST variations are investigated, using two methods. The first method is ocean mixed layer heat budget analysis. The budget diagnosis result shows that the thermodynamic processes dominate in the rapid warming phases, while the ocean dynamics dominate during the hiatus phases. The second method relies on the diagnosis of a simple equilibrium state model. This model captures well the horizontal distribution of SST difference between two warmer and cooler equilibrium states during either the rapid warming or hiatus phases. It is found that the SST difference during the rapid warming phases is primarily controlled by the increase of downward longwave radiation as both column integrated water vapor and CO_2 increase during the phases. During the hiatus phases, the water vapor induced greenhouse effect offsets the CO_2 effect, and the SST cooling tendency is primarily determined by the ocean dynamics over the Southern Ocean and tropical Pacific. The SST pattern associated with the Interdecadal Pacific Oscillation (IPO) might be responsible for the remote and local ocean dynamic responses through induced wind change.

Key words: SST trends, Natural variability, Global warming

1. Introduction

Because of anthropogenic activities, there is steady increase of greenhouse gases such as CO_2 in the atmosphere since the Industrial Revolution. The increase of the greenhouse gases (GHGs) traps more longwave radiation within the atmosphere due to the so called greenhouse effect. While the GHGs kept increasing during the past one hundred years, GMST didn't increase all the time. For instance, during the past one hundred years (say, 1910 to 2012), there are four relatively warming and cooling phases. The periods from 1910 to 1940s and from mid-1970s to 1997 are so called global rapid warming phases, whereas the period from 1940s to mid-1970s and from 1998 to 2012 are known as warming hiatus periods.

Previous studies suggested that the bigger hiatus during the period from 1940s to mid-1970s was attributed to the increasing of artificial aerosols, which resulted in a decrease of cloud particle size and an increase of cloud albedo (Lohmann and Feichter. 2005; Hateren 2012; Kosaka and Xie. 2016). Thus the cooling during that period was primarily attributed to the reduction of incoming solar radiation. Another possible factor is natural mode variability such as the IPO, which may have a far-reaching effect on GMST (Meehl et al. 2013; Kosaka and Xie. 2016). Various hypotheses have been proposed to interpret the recent hiatus phase. One is that the hiatus might be caused by data bias (Karl et al. 2015; Jones 2016). The magnitude and statistical significance of a trend depend on time intervals considered (Fyfe et al. 2016). The second hypothesis emphasizes the effect of the IPO. Anomalous heat source in the tropics associated with the IPO may force a quasi-stationary atmospheric Rossby wave response to affect higher-latitude wind and temperature (Trenberth et al. 2014). It has been argued that GMST warming stagnates during the IPO negative phases (e.g., Kosaka and Xie. 2013; England et al. 2014; Meehl et al. 2014; Trenberth 2015; Kosaka and Xie. 2016). The third hypothesis suggests that a positive Atlantic Multidecadal Oscillation (AMO) may promote a global cooling (Steinman et al. 2015). The fourth hypothesis suggests the shift of heat from the surface into the deep ocean over Indian Ocean, North Atlantic and/or Southern Ocean (Meehl et al. 2011; Chen and Tung 2014; Kintisch 2014; Roemmich et al. 2015; Lee et al. 2015; Liu et al. 2016; Li et al. 2017). Liang et al. (2017) suggested that ocean mixing processes, including isopycnal and diapycnal as well as convective mixing, are important for the decadal change of the heat exchange between upper and deeper ocean. Other hypotheses include the effect of that volcanic eruptions (Fyfe et al. 2013; Santer et al. 2014) and anthropogenic aerosols. For example, Smith et al. (2016) reckoned that the phase of the IPO during the hiatus period was modulated by external forcing of anthropogenic aerosols.

Because the ocean surface covers 71% of the earth's surface, the trend of GMST is, to a large extent, determined by that of the global mean SST. Figure 1 shows the time series of the global mean SST (blue curve) during the last one hundred years. Consistent with the GMST, there are two rapid SST warming periods and two SST cooling periods. The warming phases occurred from 1910 to 1942 (hereafter Phase 1) and from 1976 to 1997 (hereafter Phase 3), and the cooling phases happened from 1943 to 1975 (hereafter Phase 2) and from 1998 to 2012 (hereafter Phase 4). It is further noted that ocean mixed layer temperature experienced similar warming and cooling phases (see the red solid line in Fig. 1). Thus, to the first order of approximation, one may examine the ocean mixed layer temperature evolution, omitting the deeper ocean warming process.

Motivated by the results above, in this study we intend to reveal fundamental physical processes responsible for the distinctive warming and cooling trends during the four periods, based on an ocean mixed layer heat budget analysis. The objective of the current study is to quantitatively measure the relative roles of ocean dynamics (including three dimensional oceanic temperature advection) and thermodynamic processes (including shortwave radiation, longwave radiation, latent and sensible heat fluxes) in causing the warming and cooling tendencies during the different phases (Phase 1 to Phase 4) through a detailed mixed-layer heat budget analysis. Physically, the SST warming or cooling tendency is caused by many factors, include external GHG forcing, natural modes such as interdecadal variability, change of solar radiation due to artificial or volcano aerosol, and so on. Previous studies seldom paid attention to the detailed diagnosis of dynamic and thermodynamic terms that affect SST. In this study, we attempt to quantitatively assess dominant physical processes that caused the distinctive SST tendencies during the warming and cooling phases, using two complementary diagnostic methods. Through the quantitative assessment of individual SST controlling factors, one may better understand global mean SST change in the past century and tackle the global warming problem.

The remaining part of this paper is organized as following. In Section 2, we describe data and analysis methods to be used. In Section 3, we present the result from mixed layer heat budget diagnosis. Section 4 shows the result from a simple equilibrium state model. Finally, a conclusion is given in Section 5.

2. Data and method

The primary datasets used in this study include 1) monthly SST dataset from Met Office Hadley Center Version 1.1 (Rayner et al. 2003), 2) monthly ocean reanalysis data Version 2.2.4 and Version si.3 from SODA (Simple Ocean Data Assimilation) including zonal velocity, meridional velocity, vertical velocity, temperature and salinity (Giese et al. 2016), 3) monthly ocean mixed layer depth from GODAS (Global Ocean Data Assimilation System), and 4) 20^{th} century atmospheric reanalysis data Version 2c provided by NOAA-CIRES (Cooperative Institute for Research in Environmental Science) that include surface upward longwave radiation, surface downward longwave radiation, surface net shortwave radiation, surface latent heat flux, surface sensible heat flux, precipitation, surface 10m wind, multi-layer atmospheric wind and specific humidity, and cloud cover. It is worth mentioning that the SODA V2.2.4 dataset covers only from 1900 to 2008. And this SODA V2.2.4 reanalysis dataset has been widely used for ocean analysis in numerous studies (e.g., An and Choi 2013; Chen et al. 2016). In order to replenish the whole time period, we use the SODA si.3 for the period from 2009 to 2013. Both the SODA datasets are driven by 20^{th} century reanalysis ensemble mean forcing fields.

Recent studies such as Liang et al. (2017) and Ponte and Piecuch (2018) used a dynamically consistent new dataset, ECCO. But such a dataset is too short (only starting from 1992) to satisfy the purpose of the current study. To reduce the impact of data uncertainty, we developed two diagnostic methods, in order to validate the results against each. By using two different diagnostic methods, we attempt to understand the role of dynamic (including 3D ocean advection) and thermodynamic (i.e., surface heat fluxes) processes in causing the distinctive SST changes.

The first method is the diagnosis of global ocean mixed layer heat budget. The depth of ocean mixed layer is defined as the depth where ocean temperature is 0.5 degree lower than the surface temperature. Following Li et al. (2002), the ocean mixed layer temperature equation can be written as

$$\frac{\partial T}{\partial t} = -u\frac{\partial T}{\partial x} - v\frac{\partial T}{\partial y} - w\frac{\partial T}{\partial z} + \frac{Q}{\rho C H} + R \qquad (1)$$

where T, u, v, and w represent, respectively, ocean temperature, zonal current velocity, meridional current velocity and vertical current velocity fields, Q denotes the sum of surface heat flux terms including net surface longwave radiation, net surface shortwave radiation, surface latent heat flux and surface sensible heat flux, ρ = 1025kg/m^3 denotes density of the ocean, C = 4096J/(kg·K) is the specific heat of the ocean, and H is the depth of the ocean mixed layer. R is a residual term representing either the bias of the reanalysis data or sub-grid processes unresolved.

Before the budget analysis, all fields are subjected to a 5–year weighted running mean (10%, 20%, 40%, 20%, 10%). Each term in Equation 1 is integrated vertically from the surface to the depth of the ocean mixed layer. By doing so, we implicitly describe the vertical mixing in the upper ocean. The mixed layer depth varies with space in general, and is obtained from the diagnosis of the ocean reanalysis dataset GODAS. The calculated mixed layer depth is at a range of 50 to 120 meters. The left hand side of equation (1) represents ocean mixed layer temperature tendency. All budget terms in Tables 1-4 are diagnosed based on the ocean reanalysis products (ocean temperature and 3D oceanic advection) and atmosphere reanalysis products (surface heat flux). Our calculation shows that the mixed-layer temperature tendency at the left side of the equation is approximately equal to the sum of four terms at the right side of the equation for most of the warming and cooling phases. This gives us confidence to further analyze the contributions from individual terms.

The second method is based on the analysis of a simple equilibrium model, following Zhang and Li (2014). By assuming that SST at each of peaks (represented by black lines in Fig. 1) is approximately in an equilibrium state, one may derive a balance between the net surface heat flux term and the ocean dynamic term at the equilibrium state. Thus a difference between two adjacent states during either a warming or a cooling phase may be written as

$$\delta Q_{net} + \delta D_o = 0 \qquad (2)$$

In equation (2), Q_{net} denotes the net surface heat flux term that consists of upward longwave radiation, downward longwave radiation, shortwave radiation, latent heat flux and sensible heat flux at the ocean surface; D_o represents three dimensional ocean advection terms, and δ denotes the difference between two equilibrium states. Through a series of simplification, Zhang and Li (2014) finally obtained the following equation for the SST difference field between the two equilibrium states:

$$\delta T_s = \frac{\delta Q_{sw} + \delta Q_{lw}^{down} - \delta Q_{lh}^{a} - \delta Q_{sh}^{a} + \delta D_o}{4\sigma \overline{T_s}^3 + \gamma_1 \overline{Q_{lh}} + \gamma_2 \overline{V}} \quad (3)$$

In equation (3), an over-bar denotes the climatological long-term mean field and T_s is the sea surface temperature. δQ_{lh}^a and δQ_{sh}^a denote the part of surface latent and sensible heat flux change related to the change of atmospheric variables such as surface wind speed, $\sigma = 5.67 \cdot 10^{-8} W/(m^2 \cdot K^4)$ is the Stefan constant, V is the surface wind speed, and coefficients γ_1 and γ_2 are the functions of latitude only. For more detailed derivation, readers are referred to Appendix A.

3. Diagnosis of ocean mixed layer heat budget for Phase 1-4

The cause of the distinctive mixed-layer temperature tendencies during the four warming and cooling phases is addressed through an oceanic mixed layer heat budget analysis. According to equation (1), the time change rates of ocean mixed layer temperature in the four phases and throughout the entire period are diagnosed respectively. The results are shown in Table 1. Note that the sign and magnitude of the diagnosed temperature tendencies at the right side of equation (1) during each of these phases and the entire period are consistent with the observed trends. In particular, the sums of the diagnosed 3D oceanic advection terms and surface heat flux terms show a warming tendency in Phase 1 and 3 and a cooling tendency in Phase 2 and 4. While the residual terms at each phase are in general small, a relatively larger error appears in phase four. The errors are possibly due to the use of inconsistent datasets between ocean reanalysis and surface heat flux products. Nevertheless, the signs of increasing and decreasing trends during the four periods are same as the observed.

The result from Table 1 indicates that from the global mean point of view, the oceanic thermodynamic process dominates the dynamic process during the warming phases (i.e., Phase 1 and 3), whereas the ocean dynamic process dominates the thermodynamic process during the cooling phases (i.e., Phase 2 and 4). Therefore, in Phase 1 and 3, the overall ocean cooling effect due to 3D advection is weaker than the surface heat flux warming effect, whereas the opposite is true in Phase 2 and 4. Thus it is the relative strength of the dynamic and the thermodynamic effect that determines the final outcome of the global mean SST trend in a particular period. A key question then becomes what causes the change of the dynamic and thermodynamic budget terms at different phases.

It is worth mentioning that from a global mean perspective, the ocean dynamical term is always negative, while the thermodynamic term is always positive. This implies that the overall dynamic effect for the global mixed layer is cooling, while the overall thermodynamic effect for the global mixed layer is warming. Among the dynamic terms, zonal advection and vertical advection are negative, while meridional advection is positive but its magnitude is much weaker.

To understand the relative contributions of each budget term during different warming and cooling phases, we first analyze the mixed-layer heat budget for the entire period, and then we subtract the mean tendency at each phase to see the relative change. Figure 2 shows the global mean budget during the entire period (1910-2012). The overall trend is positive, because the net heat flux warming effect exceeds the ocean dynamic cooling effect. Among the various heat flux terms, the dominant contributors for the warming are downward longwave radiation (due to increased greenhouse gases) and net shortwave radiation, and the combination of the two exceeds the cooling effect induced by upward longwave radiation, surface latent and sensible heat fluxes.

Figure 4 shows long-term (1910-2012) climatological mean SST, upward and downward longwave radiation, precipitation, low cloud cover, net shortwave radiation, latent heat flux, 850hPa wind, and ocean mixed-layer temperature advection fields. It is interesting to note that both the upward and downward longwave radiative fluxes have a pattern resembling to the long-term mean SST field. The resemblance of the upward longwave radiative flux to the mean SST is not surprising, because according to Stefan's law, more upward longwave radiation emission should happen in the region where SST is warmer. The resemblance of the downward longwave radiative flux to the SST implies that the downward longwave radiative flux is more controlled by atmospheric water vapor distribution than the CO_2 distribution. The latter is more spatially uniform, while column integrated specific humidity field has a pattern similar to the mean SST field (figure not shown). As expected, the maximum warming associated with the shortwave radiation and maximum cooling associated with the surface latent heat flux all appear in the tropics. The maximum ocean dynamic effect is mainly confined over equatorial oceans, Southern Ocean and western boundary current regions.

Figure 3a shows the difference of the budget terms between the warming phases composite (i.e., Phase 1 and 3) and the entire period. Compared with the mean temperature tendency during the entire period, the warming tendency averaged for Phase 1 and 3 is about 1°C per 100 years higher. The major terms that contribute to the higher warming tendency are upward longwave radiative flux and surface latent heat flux. The cause of such changes will be discussed below, with the analysis of horizontal maps of key variables. The downward longwave radiative flux is reduced, because the CO_2 amount averaged during Phase 1 and 3 is less than that during the entire period.

During the composite warming phases (Phase 1 and 3), the SST difference field (relative to the long term mean SST) shows a positive IPO pattern, with positive SST anomalies in the tropical eastern Pacific (Fig. 5a). The rest of the global ocean is anomalous cold. Because of the SST pattern, one would expect an increased upward longwave radiative flux over the tropical east Pacific and a decreased upward longwave radiative flux elsewhere. Since the surface flux in all figures is defined positive downward, an overall global surface warming is resulted due to the change of the upward longwave radiative flux (Fig. 5b). This result is consistent with Fig. 3a, which indicates that this thermodynamic process is a dominant term contributing to the warming trend in Phase 1 and 3.

The downward longwave radiation difference filed shows a nearly globally decreasing (Fig. 5c). This is because the CO_2 amount is lower during Phase 1 and 3 than during the entire period. In addition, column integrated water vapor difference is mostly negative in the globe (figure not shown), closely following the SST pattern shown in Fig. 5a. The positive SST anomaly in the tropical eastern Pacific causes the reduction of trade wind in the Pacific, which on one hand suppresses the ocean upwelling and leads to a positive ocean dynamic contribution in the equatorial Pacific (Table 2), and on the other hand reduces surface latent heat flux and leads to a thermodynamic warming (Fig. 5g).

The precipitation field (Fig. 5d) shows an increase in tropical central Pacific and a decrease in the Maritime Continent. It is likely that this anomalous heating pattern is responsible for generating anomalous easterlies over Southern Ocean and anomalous westerlies over the equatorial Atlantic (Fig. 5g). The former is through energy dispersion of a stationary Rossby wave train in response to the tropical heating (Hoskins and Karoly 1981). The latter is through anomalous Walker Circulation, which suppresses convection over Amazon (García-Serrano et al. 2017). The change of the wind in Southern Ocean may cause the SST warming through reduced ocean vertical mixing and surface latent heat flux as the mean wind is westerly. The anomalous westerly in the equatorial Atlantic may induce warming through positive horizontal and vertical advection anomalies.

To assess the relative contribution of ocean dynamics in different basins, the global ocean is divided into six basins, namely, tropical Pacific (30°S-30°N, 120°E-80°W), tropical Atlantic (30°S-30°N, 80°W-0°W), tropical Indian Ocean (30°S-20°N, 40°E-100°E), Southern Ocean (60°S-30°S, 0°E-0°W), north Pacific (30°N-60°N, 130°E-120°W) and north Atlantic (30°N-60°N, 80°W-10°W). Table 2 shows the area averaged ocean advection terms and area percentage at each of these basins. The product of each term value and area percentage may be regarded as actual contribution of the term at the basin to the global ocean dynamical tendency. Thus Table 2 shows that the most important basins for the ocean dynamic contribution are Southern Ocean and tropical Pacific, followed by tropical Atlantic. Keep in mind that such a dynamic warming shown in Table 2 is relative to the overall dynamic cooling effect averaged throughout the entire period. Such a dynamic impact appears crucial in causing the rapid warming trend during Phase 1 and 3 (Fig. 3a).

The cause of the dynamic warming is attributed to both the remote and local wind responses to the tropical Pacific SST anomaly, which is closely related to the SST variability associated with the IPO. Thus the mixed layer heat budget analysis results above support the notion that it is the natural variability that plays an important role in regulating the global mean SST variation in different stages, in addition to CO_2 induced upward warming trend.

It is worth mentioning that an additional process related to low-level stratus cloud response may partially contribute to the warming trend during Phase 1 and 3. In response to the warm SST anomaly in the tropical eastern Pacific, the amount of low-level stratus cloud is reduced in the eastern equatorial Pacific due to reduced atmospheric static stability (Li and Philander 1996, Li 1997). The decrease of the low-level stratus cloud amount may further increase net downward shortwave radiation, contributing to an additional warming in Phase 1 and 3.

A nearly mirror image is found in the mixed layer heat budget difference terms between the composite cooling phases (i.e., Phase 2 and 4) and the entire period (Fig. 3b). Figure 6 shows the horizontal patterns of the average SST, wind, precipitation and heat flux difference fields between the composite cooling phases (i.e., Phase 2 and 4) and the entire period. These patterns are in general opposite to those for the composite warming phases shown in Fig. 5. A cold SST anomaly appears in the tropical eastern Pacific. The overall SST pattern in the Pacific resembles a typical negative phase of the IPO (Fig. 6a). Upward (downward) longwave radiation field shows a nearly globally decreasing (increasing) (Fig. 6b, c). In the 850hPa wind field, anomalous westerlies appear in the Southern Ocean, and they enhance the climatological westerly and increase the local ocean vertical mixing and surface latent heat flux (Fig. 6g, h). Anomalous easterlies appear in the tropical Pacific and Atlantic in response to the negative phase of IPO, and strengthen both the surface latent heat flux and the oceanic advective cooling (Fig. 6g, h), leading to the overall SST cooling trend during the phases (Fig. 3b). Low stratus cloud amount in tropical eastern Pacific increases, which contributes to the decrease of local surface shortwave radiation (Fig. 6f).

As shown in Fig. 3b, the ocean dynamics play a crucial role in causing the cooling trend during Phase 2 and 4. Table 3 shows the relative contribution of the ocean dynamic terms at each basin. Consistent with the result shown in Fig. 6h, the most important ocean basins that contribute to the cooling trend are the Southern Ocean, tropical Pacific, and tropical Atlantic.

4. Results from a simple equilibrium state model

In the previous section, we compare the mixed-layer temperature tendencies averaged at each phase. Taking a different approach, we now focus on examining fundamental processes that cause SST difference between two adjacent equilibrium warmer and cooler states. As illustrated by black lines in Fig. 1, five such equilibrium states are selected. They are named as E1 (1903-1912), E2 (1937-1946), E3 (1965-1976), E4 (1997-1999), and E5 (2011-2013). For example, by diagnosing equation (3) between E2 and E1, one may reveal the relative contribution of each term in the right hand side of the equation to the SST difference between E2 and E1. The average period for each equilibrium state is 10 years, except for the last two due to the fact that the latest hiatus period is relatively short. Figure 7 shows the diagnosis result for composite warming and cooling phases, respectively. The warming phases consist of the SST difference between E2 and E1 and between E4 and E3, and the cooling phases consist of the SST difference between E3 and E2 and between E5 and E4.

The first bar in Fig. 7a shows the observed global mean SST change during the composite warming phases (Phase 1 and 3). The observed global average SST difference is 0.3°C. The second bar in Fig. 7a shows the diagnosed result based on the sum of all terms (including the ocean dynamic contribution and various heat flux terms) at the right hand side of equation (3). The diagnosed SST change agrees well with the observed SST change.

The marked warming in Phase 1 and 3 is primarily attributed to the increase of downward longwave radiation (δQ_{lw}^{down}) and wind induced surface latent heat flux change (δQ_{lh}^{a}) (Fig. 7a). To understand the cause of such changes, we further examine the horizontal patterns of composite SST, wind, humidity and heat flux difference fields. Figures 8a and 8b show the SST difference patterns from the observation and the diagnosis based on equation (3). The two patterns are almost identical, indicating that the simple equilibrium state model is able to capture the global SST changes. A general warming appears everywhere except in north Pacific (near the Kurishio extension region). Superposed on a uniform warming pattern is a positive IPO pattern, with a maximum warming appearing in the equatorial eastern Pacific. It appears that the SST difference pattern shown in Fig. 8a is the sum of a global uniform warming pattern and a positive-phase IPO.

The SST warming pattern leads to the increase of column integrated specific humidity in most of global atmosphere (Fig. 8d), possibly through enhanced surface evaporation (due to reduced sea-air specific humidity difference) and the increase of SST induced atmospheric convection and precipitation (Fig. 8f). The increased column integrated water vapor, working together with increased CO_2, causes a marked increase of downward longwave radiative flux (Fig. 8c), which further warms the SST.

A greater warming in the equatorial eastern Pacific associated with the IPO induces anomalous low-level westerlies over the equatorial central Pacific (Fig. 8e), which in turn helps strengthen the eastern Pacific warming through induced ocean advective processes (figure not shown). The westerly wind anomaly also helps warm the equatorial ocean through the reduced surface latent heat flux (Fig. 8e).

To sum up, the SST difference between two equilibrium states (E2 minus E1 and E4 minus E3) is primarily caused by the increase of downward longwave radiation due to the increase of both the atmospheric water vapor and CO_2, and the decrease of wind induced surface latent heat flux.

Fig. 7b shows a parallel diagnosis for the SST difference between two equilibrium states during the cooling phases. The global mean SST difference is about -0.05°C, weaker than its counterpart during the warming phases. Again the diagnosed SST difference based on the simple equilibrium state model is close to the observed value. Different from the warming phases, the cooling is primarily caused by the strengthened ocean dynamic cooling effect and the decrease of the downward longwave radiation (Fig. 7b).

To reveal physical processes responsible for the aforementioned changes, we examine the horizontal patterns of composite SST, wind, heat flux, and ocean advection difference fields. The major SST cooling appears in the tropical Pacific, tropical Atlantic and tropical Indian Ocean (Fig. 9a). The SST difference pattern in the Pacific resembles a negative-phase IPO. During the cooling phases, the column integrated specific humidity decreases in most of the globe (Fig. 9d). As a result, the greenhouse effect due to the change of water vapor tends to be against that due to the change of CO_2. On other words, although CO_2 kept on increasing during the cooling phases, the warming effect due to CO_2 was somewhat offset by the cooling effect due to the decrease of atmospheric water vapor. The net effect of the two GHGs is the decrease of downward longwave radiation, as shown in Figs. 9c and 7b.

The most important cooling mechanism during Phase 2 and 4 arises from the ocean dynamics (Fig. 7b). There are two ways to calculate the ocean dynamic contribution. One is indirectly estimated based on the global net surface heat flux contribution (Zhang and Li 2014). Another is the direct diagnosis of the global ocean 3D advection terms (such as those done in Section 3). Both the results are presented in Fig. 7, with “D” denoting the result from the heat flux estimation and “diag_D” denoting the result from the direct ocean advection calculation. The results are quite consistent. In response to a cold SST anomaly in eastern equatorial Pacific, easterly anomalies appear in the equatorial central Pacific (Fig. 9e). The anomalous easterlies enhance ocean upwelling and cold zonal advection along the equatorial Pacific. The enhanced Walker circulation also induces positive rainfall anomalies over the Maritime Continent (Fig. 9f), which may, through remote teleconnection, induce circulation anomalies in higher latitudes in such a way that there are anomalous cyclonic centers over the Southern Ocean between 30°E and 90°E and between 70°W and 30°W (Fig. 9e). The low-level cyclonic wind anomalies in the regions tend to enhance ocean upwelling, favoring a cooling there (Fig. 10).

Table 4 shows the relative contributions of the diagnosed ocean dynamical processes at each basin to the global SST cooling during Phase 2 and 4. The values shown in Table 4 are just area average. Given much greater percentage area in the Southern Ocean and tropical Pacific, the main contributors for the ocean dynamic cooling arise from the Southern Ocean and tropical Pacific. The overall result here seems consistent with that in section 3 with use of Method 1, that is, the ocean dynamics plays a more important, vital role during the cooling phases whereas the thermodynamic process dominates during the warming phases. It is also consistent with the recent study by Yao et al. (2017), who emphasized the role of tropical Pacific Ocean in the recent hiatus phase.

5. Conclusion

In the past 100 years, the global mean SST exhibits four distinctive warming and cooling phases. The specific dynamic and thermodynamic processes that determine the relative warming and cooling tendencies are investigated through the diagnosis of the ocean mixed layer heat budget. It is found that the ocean thermodynamic process dominates during the warming phases, whereas the ocean dynamic process dominates during the cooling phases. Removing the long term tendency, the relative warming or cooling phases are primarily determined by the ocean dynamic effect. While the relative warming trend arises from a weakened ocean dynamic cooling effect, a relative cooling trend results from an enhanced ocean dynamic effect.

A further analysis shows that the mean state during the relative warming phase resembles a positive IPO phase, with a positive SST anomaly in the tropical eastern Pacific and negative SST anomalies elsewhere. Such a SST pattern results the overall decrease of upward longwave radiative flux, favoring the surface warming. Meanwhile, the IPO induced westerly anomalies over the equatorial Pacific cause a warming tendency through both the ocean dynamics and surface latent heat flux change. The IPO induced tropical heating also generates a remote wind response in the Southern Ocean, which favors a dynamic warming in the region. Similarly, a strengthened dynamic cooling effect happens in the same regions during the cooling phases.

While the mixed-layer heat budget analysis above focused on the relative roles of ocean dynamic (3D advection) and thermodynamic (heat flux) processes in causing the distinctive warming and cooling tendencies at each phase, in the second method we focus on examining the cause of the SST difference between two equilibrium states during either a warming or a cooling phase. Thus this diagnosis approach focuses only on the process difference between the two equilibrium states, neglecting any processes between the two states. Our calculation shows that the simple equilibrium model is able to capture the observed SST difference in each of the four relative warming and cooling phases. It is found that the composite warming is attributed to the increase of downward longwave radiation due to the increase of both the column integrated water vapor and CO_2, and the decrease of upward latent heat flux due to reduced wind speed associated with the SST change. The composite cooling, on the other hand, is a combined result of enhanced ocean dynamic cooling, in particular over the Southern Ocean and tropical Pacific, and reduced downward longwave radiation. The latter is attributed to the decrease of column integrated water vapor, even though CO_2 continues increasing.

While the two analysis methods emphasize different aspects of atmospheric and oceanic processes in regulating the global SST tendency, they are complementary each other. Method 1 concentrates on processes affecting the mixed-layer temperature tendencies at each of the warming and cooling phases, whereas Method 2 focuses on the cause of the SST difference between a warmer and a cooler equilibrium states, neglecting processes in between. Through the two methods, we do come up with a consistent conclusion, that is, the ocean dynamics appear dominant during the cooling phases, while the surface heat flux, particularly latent heat flux and water vapor modulated downward longwave radiative flux, play a more important role during the warming phases. The most important regions for the ocean dynamic effect are the Southern Ocean and tropical Pacific.

A caution is needed in interpreting some of the current results as the current study uses various datasets from different sources and there is uncertainty and inconsistence among these datasets. A longer and more accurate dataset is needed for such a trend analysis.

Previously a number of studies were conducted in understanding the hiatus of global mean SST since 2000 and the decrease trend in 1950-70s. For instance, some suggested that the hiatus in recent decade was a result of tropical Pacific forcing in conjunction with the Interdecadal Pacific Oscillation (IPO) (e.g., Kosaka and Xie 2013; Yao et al. 2017). Others suggested that the recent hiatus was a result of more heat stored in the deep ocean (e.g., Chen and Tung 2014; Liu et al. 2016; Roemmich et al. 2017), while the previous hiatus was caused by volcanic forcing (e.g., Fyfe et al.2013; Santer et al. 2014). The results from the current study are complementary to these previous results. For instance, during the hiatus phases, the water vapor induced greenhouse effect associated with the IPO offsets the CO_2 effect, indicating the importance of the nature variability in regulating global SST trend during the periods. Our diagnosis shows that the ocean dynamics over the Southern Ocean associated with remote IPO wind forcing is important in promoting a negative SST trend during the hiatus phases. Compared to the recent hiatus period, the net surface shortwave radiation is smaller due to greater volcanic effect during the previous cooling phase, as inferred from Table 1. Thus there is a need to carefully separate the natural and anthropogenic effects on the GMST evolution.

Appendix A: An Equilibrium State Model for SST Change

By Stefan's law, the change of upward longwave radiation at the ocean surface may be approximately written as

$$\delta Q_{lw}^{up} = 4\sigma \overline{T_s}^3 \delta T_s$$

The bulk formulas of surface latent and sensible heat fluxes may be written as

$$Q_{lh} = \rho L C_E V(q_s - q_a) = \rho L C_E V(1 - \mathrm{RH} e^{-\alpha \Delta T}) q_s$$

and

$$Q_{sh} = \rho C_H C_P V(T_s - T_a) = \rho C_H C_P V \Delta \mathrm{T}$$

where ρ is air density near the surface, C_E and C_H are the heat exchange coefficient of Q_{lh} and Q_{sh}, C_P is the specific heat capacity at constant pressure, and $\Delta \mathrm{T}$ is the difference between SST and surface air temperature.

The change of Q_{lh} with respect to change of SST may be written as

$$\delta Q_{lh}^{o} = \frac{\partial Q_{lh}}{\partial q_s}\frac{\partial q_s}{\partial T_s}\delta T_s = \frac{L_v}{R\overline{T_s}^2}\overline{Q_{lh}}\delta T_s = \gamma_1 \overline{Q_{lh}} \delta T_s$$

where L_v is the latent heat of condensation and R is the ideal gas constant for water vapor. The notation $\delta Q_{lh}^{a} = \delta Q_{lh} - \delta Q_{lh}^{o}$ denotes the part of surface latent heat flux change due to the change of atmospheric wind speed, relative humidity and air-sea temperature difference. Similarly, Q_{sh} can be decomposed as

$$\delta Q_{sh}^{o} = \frac{\partial Q_{sh}}{\partial \Delta \mathrm{T}} \frac{\partial \Delta \mathrm{T}}{\partial T_s} \delta T_s = \rho C_H C_P \bar{V} \delta T_s = \gamma_2 \bar{V} \delta T_s$$

where $\partial \Delta \mathrm{T} / \partial T_s$ is determined based on the linear relationship between $\Delta \mathrm{T}$ and T_s in the present-day climate state. By substituting each of the flux terms into equation (2), one can obtain:

$$\delta Q_{sw} - 4\sigma \bar{T_s}^3 \delta T_s + \delta Q_{lw}^{down} - \gamma_1 \overline{Q_{lh}} \delta T_s - \delta Q_{lh}^{a} - \gamma_2 \bar{V} \delta T_s - \delta Q_{sh}^{a} + \delta D_0 = 0$$

Thus, the change of SST, δT_s, can be diagnosed by transforming the equation above into equation (3).

Acknowledgments. We thank the anonymous reviewers for their constructive comments that greatly improve the original manuscript. This work is jointly supported by China National Key R&D Program 2017YFA0603802 and 2015CB453201, NSFC grants 41630423 and 41875069, NSF grant AGS-1565653, and NOAA grant NA18OAR4310298. This is SOEST contribution number 12345, IPRC contribution number 1234 and ESMC number 123.

References

An, S-I, Choi, J., 2013. Inverse relationship between the equatorial eastern Pacific annual-cycle and ENSO amplitudes in a coupled general circulation model. Clim. Dyn 40, 663–675.

Chen, L., Yu, Y., Zheng, W., 2016. Improved ENSO simulation from climate system model fgoals-g1.0 to fgoals-g2. Clim. Dyn 47(7-8), 2617-2634.

Chen, X., Tung, K. K., 2014. Varying planetary heat sink led to global-warming slowdown and acceleration. Science 345(6199), 897-903.

England, M. H., Mcgregor, S., Spence, P., Meehl, G. A., Timmermann, A., Cai, W., Gupta, A. S., Mcphaden, M. J., Purich, A., Santoso, A., 2014. Recent intensification of wind-driven circulation in the pacific and the ongoing warming hiatus. Nat. Clim. Change 4(3), 222-227.

Fyfe, J. C., Gillett, N. P., Zwiers, F. W., 2013. Overestimated global warming over the past 20 years. Nat. Clim. Change 3(9), 767-769.

Fyfe, J. C., Meehl, G. A., England, M. H., Mann, M. E., Santer, B. D., Flato, G. M., Hawkins, E., Gillett, N. P., Xie, S. P., Kosaka, Y., Swart, N. C., 2016. Making sense of the early-2000s warming slowdown. Nat. Clim. Change 6(3), 224-228.

Giese, B. S., Seidel, H. F., Compo, G. P. Sardeshmukh, P. D., 2016. An ensemble of ocean reanalysis for 1815-2013 with sparse observational input. J. Geophys. Res. Oceans. 121, 6891-6910.

García-Serrano, J., Cassou, C., Douville, H., Giannini, A., Doblas-Reyes, F. J., 2017. Revisiting the ENSO Teleconnection to the Tropical North Atlantic. J.

Clim. 30(17), 6945-6957.

Hateren, J. H. V., 2012. A fractal climate response function can simulate global average temperature trends of the modern era and the past millennium. Clim. Dyn 40(11-12), 2651-2670.

Hoskins, B. J., Karoly, D. J., 1981. The Steady Linear Response of a Spherical Atmosphere to Thermal and Orographic Forcing. J. Atmos. Sci. 38(6), 1179-1196.

Jones, P., 2016. The reliability of global and hemispheric surface temperature records. Adv. Atmos. Sci. 33(3), 269-282.

Karl, T. R., Arguez, A., Huang, B., Lawrimore, J. H., Mcmahon, J. R., Menne, M. J., Peterson, T. C., Vose, R. S., Zhang, H. M., 2015. Possible artifacts of data biases in the recent global surface warming hiatus. Science 348(6242), 1469-1472.

Kintisch, E., 2014. Is Atlantic holding earth's missing heat? Science 345(6199), 860-861.

Kosaka, Y., Xie, S. P., 2013. Recent global-warming hiatus tied to equatorial Pacific surface cooling. Nature 501(7467), 403.

Kosaka, Y., Xie, S. P., 2016. The tropical Pacific as a key pacemaker of the variable rates of global warming. Nat. Geosci. 9(9).

Lee, S. K., Park, W., Baringer, M. O., Gordon, A. L., Huber, B., Liu, Y., 2015. Pacific origin of the abrupt increase in Indian Ocean heat content during the warming hiatus. Nat. Geosci. 8(6), 445-449.

Li, T., 1997. Air-sea interactions of relevance to the ITCZ: the analysis of coupled instabilities and experiments in a hybrid coupled GCM. J. Atmos. Sci. 54(1), 134-147.

Li, T., Y. S. Zhang, E. Lu, D. Wang, 2002. Relative role of dynamic and thermodynamic processes in the development of the Indian Ocean dipole: An OGCM diagnosis. Geophys. Res. Lett. 29(23), 2110-2113.

Li, Y., Han, W., Zhang, L., 2017. Enhanced decadal warming of the southeast Indian ocean during the recent global surface warming slowdown. Geophys. Res. Lett. 44(19).

Liang, X., Piecuch, C. G., Rui, M. P., Forget, G., Wunsch, C., Heimbach, P., 2017. Change of the global ocean vertical heat transport over 1993-2010. J. Clim. 30(14), 5319-5327.

Liu, W., Xie, S. P., Lu, J., 2016. Tracking ocean heat uptake during the surface warming hiatus. Nat. Communications 7, 10926.

Lohmann, U., Feichter, J., 2005. Global indirect aerosol effects: a review. Atmos. Chemis. & Phys. 5(3), 715-737.

Meehl, G. A., Arblaster, J. M., Fasullo, J. T., Hu, A., Trenberth, K. E., 2011. Model-based evidence of deep-ocean heat uptake during surface-temperature hiatus periods. Nat. Clim. Change 1(7), 360-364.

Meehl, G. A., Hu, A., Arblaster, J. M., Fasullo, J., Trenberth, K. E., 2013. Externally forced and internally generated decadal climate variability associated with the interdecadal pacific oscillation. J. Clim. 26(18), 7298-7310.

Meehl, G. A., Teng, H., Arblaster, J. M., 2014. Climate model simulations of the observed early-2000s hiatus of global warming. Nat. Clim. Change 4(10), 898-902.

Philander, S. G. H., D. Gu, D. Halpern, G. Lambert, N.-C. Lau, T. Li, R. Pacanowski, 1996. Why the ITCZ is mostly north of the equator. J. Clim, 9, 2958-2972.

Ponte, R. M., Piecuch, C. G., 2018. Mechanisms controlling global mean sea surface temperature determined from a state estimate. Geophys. Res. Lett. 45, 3221-3227.

Rayner, N. A., Parker, D. E., Horton, E. B., Folland, C. K., Alexander, L. V., Rowell, D. P., Kent, E. C., Kaplan, A., 2003. Global analyses of sea surface temperature, sea ice, and night marine air temperature since the late nineteenth century. J. Geophys. Res. Atmos. 108 (14), 1063-1082.

Roemmich, D., Church, J., Gilson, J., Monselesan, D., Sutton, P., Wijffels, S., 2015. Unabated planetary warming and its ocean structure since 2006. Nat. Clim. Change 2(3), 240-245.

Santer, B. D., Bonfils, C., Painter, J. F., Zelinka, M. D., Mears, C., Susan, S., Schmidt, G. A., Fyfe, J. C., Cole, J. N. S., Nazarenko, L., Taylor, K. E., Wentz, F. J., 2014. Volcanic contribution to decadal changes in tropospheric temperature. Nat. Geosci. 7(3), 185-189.

Smith, D. M., Booth, B. B. B., Dunstone, N. J., Eade, R., Hermanson, L., Jones, G. S., Scaife, A. A., Sheen, K. L., Thompson, Vikki, 2016. Role of volcanic and anthropogenic aerosols in the recent global surface warming slowdown. Nat. Clim. Change 6(10), 936-941.

Steinman, B. A., Mann, M. E., Miller, S. K., 2015. Atlantic and Pacific multidecadal oscillations and Northern Hemisphere temperatures. Science 347(6225), 988-991.

Trenberth, K. E., Fasullo, J. T., Branstator, G. Phillips, A. S., 2014. Seasonal aspects of the recent pause in surface warming. Nat. Clim. Change 4(10), 911-916.

Trenberth, K. E., 2015. Has there been a hiatus? Science 349(6249), 691-692.

Yao, S. L., Luo, J. J., Huang, G., Wang, P., 2017. Distinct global warming rates tied to multiple ocean surface temperature changes. Nat. Clim. Change 7(7), 486-491.

Zhang, L., Li, T., 2014. A simple analytical model for understanding the formation of sea surface temperature patterns under global warming. J. Clim. 27(22), 8413-8421.

Table Captions

Table 1 Ocean mixed layer dynamic and thermodynamic tendency terms during each warming and cooling phase and the entire analysis period (1910-2012). D denotes the sum of three dimensional ocean advection terms. Sum denotes the sum of the ocean dynamics term and the heat flux term. R denotes the residual term representing missing physics in the budget. Unit: ˚C/decade

Table 2 Area-averaged three dimensional advection terms (unit: °C/decade) and their sum (Dyn) during the composite SST warming phases and area percentage for each of the six ocean basins, Tropical Pacific, Tropical Atlantic, Indian Ocean, Southern Ocean, North Pacific and North Atlantic. All tendencies have been subtracted from their long-term mean values.

Table 3 Same as Table 2 except for the composite SST cooling phases.

Table 4 Composite differences of the basin-averaged ocean advection terms and their sum (Dyn) (unit: °C/decade) between two adjacent cooler and warmer equilibrium states during Phase 2 and 4 with Method 2.

Figure captions

Fig. 1 Time series with 5-year weighted running mean (10%, 20%, 40%, 20%, 10%) of the global mean SST (blue) and the global mean mixed layer temperature (red). The long-term mean SST and mixed layer temperature have been subtracted. Dotted lines separate four temperature change phases with Phase 1 from 1910 to 1942, Phase 2 from 1943 to 1975, Phase 3 from 1976 to 1997, and Phase 4 from 1998 to 2012. The correlation coefficient (CC) between the SST and mixed layer temperature time series is 0.84. Black solid lines denote five equilibrium states to represent four warming and cooling phases in Section 4.

Fig. 2 The observed and diagnosed ocean mixed layer heat budget terms (unit: °C/mon.) for the entire analysis period (1910-2012). Tt represents the temperature tendency. Term Dyn is the sum of three dimensional advection terms, including zonal advection (-uTx), meridional advection (-vTy) and vertical advection (-wTz). Term Q is the sum of five heat flux terms including upward longwave radiation (ULW), downward longwave radiation (DLW), net shortwave radiation (SW), latent heat flux (LH) and sensible heat flux (SH) at the ocean surface. "Sum" denotes the sum of Dyn and Q.

Fig. 3 Same as Fig. 2 except for (a) the composite warming phases and (b) the composite cooling phases. The long-term (1910-2012) mean tendency has been removed.

Fig. 4 Horizontal distributions of long-term (1910-2012) mean fields of (a) SST (°C), (b) upward longwave radiation (W/m^2), (c) downward longwave radiation

(W/m^2), (d) precipitation (kg/m^2/day), (e) low cloud cover (%), (f) net shortwave radiation (W/m^2), (g) surface latent heat flux (W/m^2) and 850hPa wind (m/s), and (h) the sum of three dimensional ocean advection terms (°C/mon).

Fig. 5 Same as Fig. 4 except for the difference between the composite warming phases and the long-term mean.

Fig. 6 Same as Fig. 4 except for the difference between the composite warming phases and the long-term mean.

Fig. 7 (a) The observed and diagnosed global mean SST difference (unit: °C.) averaged between E2 and E1 and between E4 and E3 and contributions from each term in the right hand side of equation (3). The first column is the observed SST difference. deltT_s denotes the diagnosed SST difference, which is sum of all terms in the right hand side of equation (3). SW denotes net shortwave radiation, DLW denotes downward longwave radiation, LHA and SHA denote wind induced latent and sensible heat flux terms δQ_{lh}^{a} and δQ_{sh}^{a} , D is the ocean dynamic term derived based on the net heat flux, and diag_D is the ocean dynamic term calculated based on 3D ocean advection. (b) Same as (a) except for the composite average between E3 and E2 and between E5 and E4.

Fig. 8 Horizontal distributions of difference fields averaged between E2 and E1 and between E4 and E3 of (a) observed and (b) diagnosed SST (°C), (c) downward longwave radiation term (°C), (d) column integrated (1000-100hPa) specific humidity (%), (e) wind induced latent heat flux term (°C) and 850hPa wind (m/s), (f) net shortwave radiation term (°C, shaded) and precipitation (kg/m^2/day, contour, with solid lines representing positive values). All heat flux terms above are calculated based on the right hand side of equation (3) and have a unit of °C.

Fig. 9 Same as Fig. 8 except for the composite difference between E3 and E2 and between E5 and E4 during the cooling phases.

Fig. 10 Same as Fig. 9 except for the difference of the three dimensional ocean advection term (°C).

Table 1 Ocean mixed layer dynamic and thermodynamic tendency terms during each warming and cooling phase and the entire analysis period (1910-2012). D denotes the sum of three dimensional ocean advection terms. Sum denotes the sum of the ocean dynamics term and the heat flux term. R denotes the residual term representing missing physics in the budget. Unit: ˚C/decade

	$\frac{\partial MixT}{\partial t}$	Sum	$-u\frac{\partial T}{\partial x}$	$-v\frac{\partial T}{\partial y}$	$-w\frac{\partial T}{\partial z}$	D	$\frac{Q}{\rho CH}$	R
Phase1	0.18	0.21	-3.30	0.43	-5.05	-7.92	**8.13**	-0.03
Phase2	-0.09	-0.10	-3.59	0.56	-4.97	**-8.00**	7.90	0.01
Phase3	0.12	0.16	-4.75	1.44	-4.86	-8.17	**8.33**	-0.04
Phase4	-0.06	-0.12	-4.98	0.77	-5.15	**-9.36**	9.24	0.06
Total	0.05	0.05	-3.95	0.74	-5.00	-8.21	**8.26**	0.00

Table 2 Area-averaged three dimensional advection terms (unit: °C/decade) and their sum (Dyn) during the composite SST warming phases and area percentage for each of the six ocean basins, Tropical Pacific, Tropical Atlantic, Indian Ocean, Southern Ocean, North Pacific and North Atlantic. All tendencies have been subtracted from their long-term mean values.

(°C/decade)	**Dyn**	**Area percentage**	$-u\frac{\partial T}{\partial x}$	$-v\frac{\partial T}{\partial y}$	$-w\frac{\partial T}{\partial z}$
Tropical Pacific	**0.38**	30%	-0.05	0.29	0.14
Tropical Atlantic	0.21	12%	-0.24	0.21	0.24
Indian Ocean	-0.26	12%	-0.49	0.07	0.16
Southern Ocean	**0.49**	32%	0.06	0.57	-0.14
North Pacific	-0.35	8%	-0.55	0.16	0.04
North Atlantic	0.07	6%	1.34	-1.11	-0.16

Table 3 Same as Table 2 except for the composite SST cooling phases.

(°C/decade)	**Dyn**	**Area percentage**	$-\mathbf{u}\frac{\partial \mathbf{T}}{\partial \mathbf{x}}$	$-\mathbf{v}\frac{\partial \mathbf{T}}{\partial \mathbf{y}}$	$-\mathbf{w}\frac{\partial \mathbf{T}}{\partial \mathbf{z}}$
Tropical Pacific	**-0.34**	30%	0.06	-0.31	-0.09
Tropical Atlantic	-0.18	12%	0.27	-0.24	-0.21
Indian Ocean	0.19	12%	0.46	-0.08	-0.19
Southern Ocean	**-0.54**	32%	-0.04	-0.61	0.11
North Pacific	0.34	8%	0.58	-0.18	-0.06
North Atlantic	-0.08	6%	-1.40	1.15	0.17

Table 4 Composite differences of the basin-averaged ocean advection terms and their sum (Dyn) (unit: °C/decade) between two adjacent cooler and warmer equilibrium states during Phase 2 and 4 with Method 2.

(°C/decade)	**Dyn**	$-u\frac{\partial T}{\partial x}$	$-v\frac{\partial T}{\partial y}$	$-w\frac{\partial T}{\partial z}$
Tropical Pacific	**-3.05**	-1.12	-0.83	-1.10
Tropical Atlantic	-1.09	-1.26	-0.49	0.66
Indian Ocean	1.06	1.22	-1.30	1.14
Southern Ocean	**-4.46**	-1.56	-2.19	-0.71
North Pacific	0.50	-2.92	3.44	-0.02
North Atlantic	-2.95	1.41	-4.16	-0.20

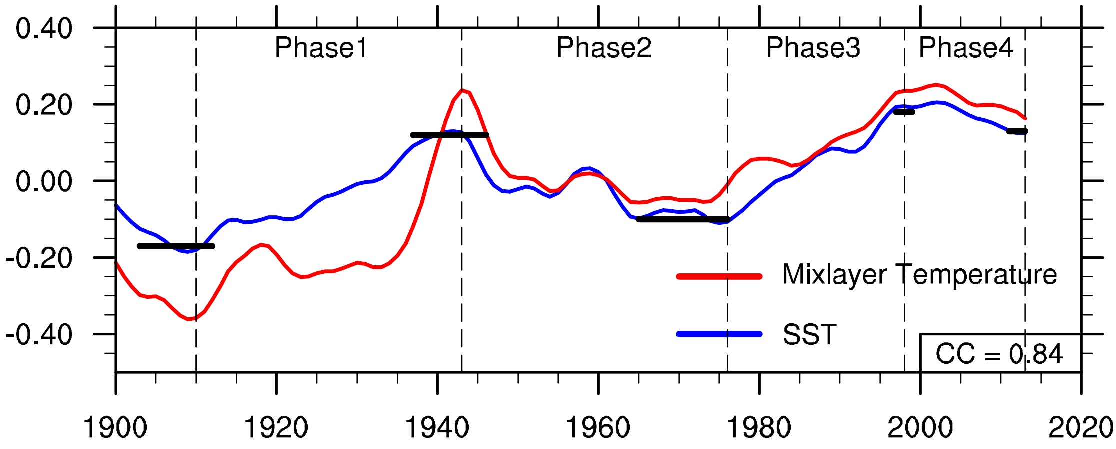

Fig. 1 Time series with 5-year weighted (10%, 20%, 40%, 20%, 10%) running mean of the global mean SST (blue) and the global mean mixed layer temperature (red). The long-term mean SST and mixed layer temperature have been subtracted. Dotted lines separate four temperature change phases with Phase 1 from 1910 to 1942, Phase 2 from 1943 to 1975, Phase 3 from 1976 to 1997, and Phase 4 from 1998 to 2012. The correlation coefficient (CC) between the SST and mixed layer temperature time series is 0.84. Black solid lines denote five equilibrium states to represent four warming and cooling phases in Section 4.

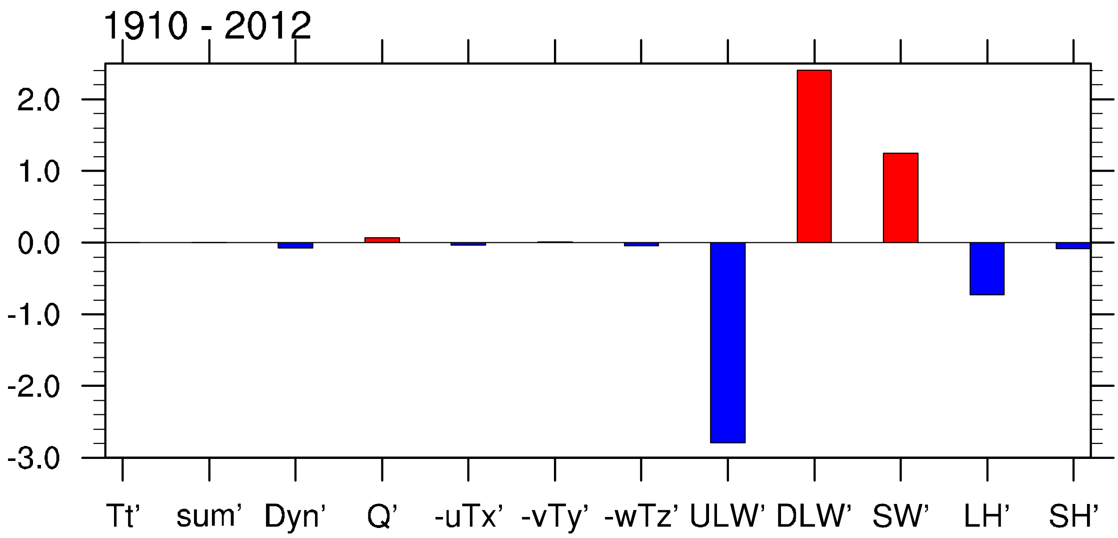

Fig. 2 The observed and diagnosed ocean mixed layer heat budget terms (unit: °C/mon.) for the entire analysis period (1910-2012). Tt represents the temperature tendency. Term Dyn is the sum of three dimensional advection terms, including zonal advection (-uTx), meridional advection (-vTy) and vertical advection (-wTz). Term Q is the sum of five heat flux terms including upward longwave radiation (ULW), downward longwave radiation (DLW), net shortwave radiation (SW), latent heat flux (LH) and sensible heat flux (SH) at the ocean surface. “Sum” denotes the sum of Dyn and Q.

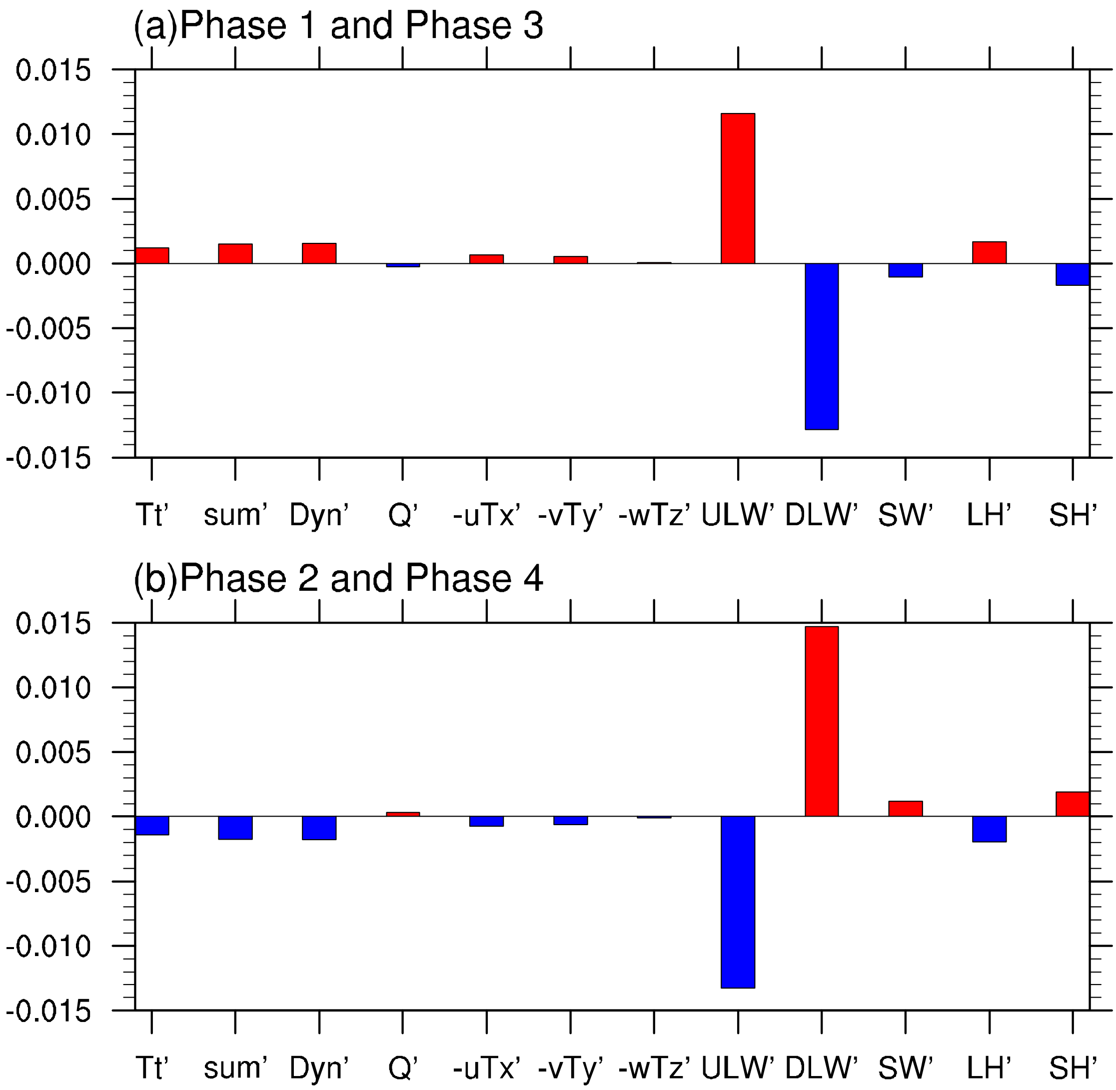

Fig. 3 Same as Fig. 2 except for (a) the composite warming phases and (b) the composite cooling phases. The long-term (1910-2012) mean tendency has been removed.

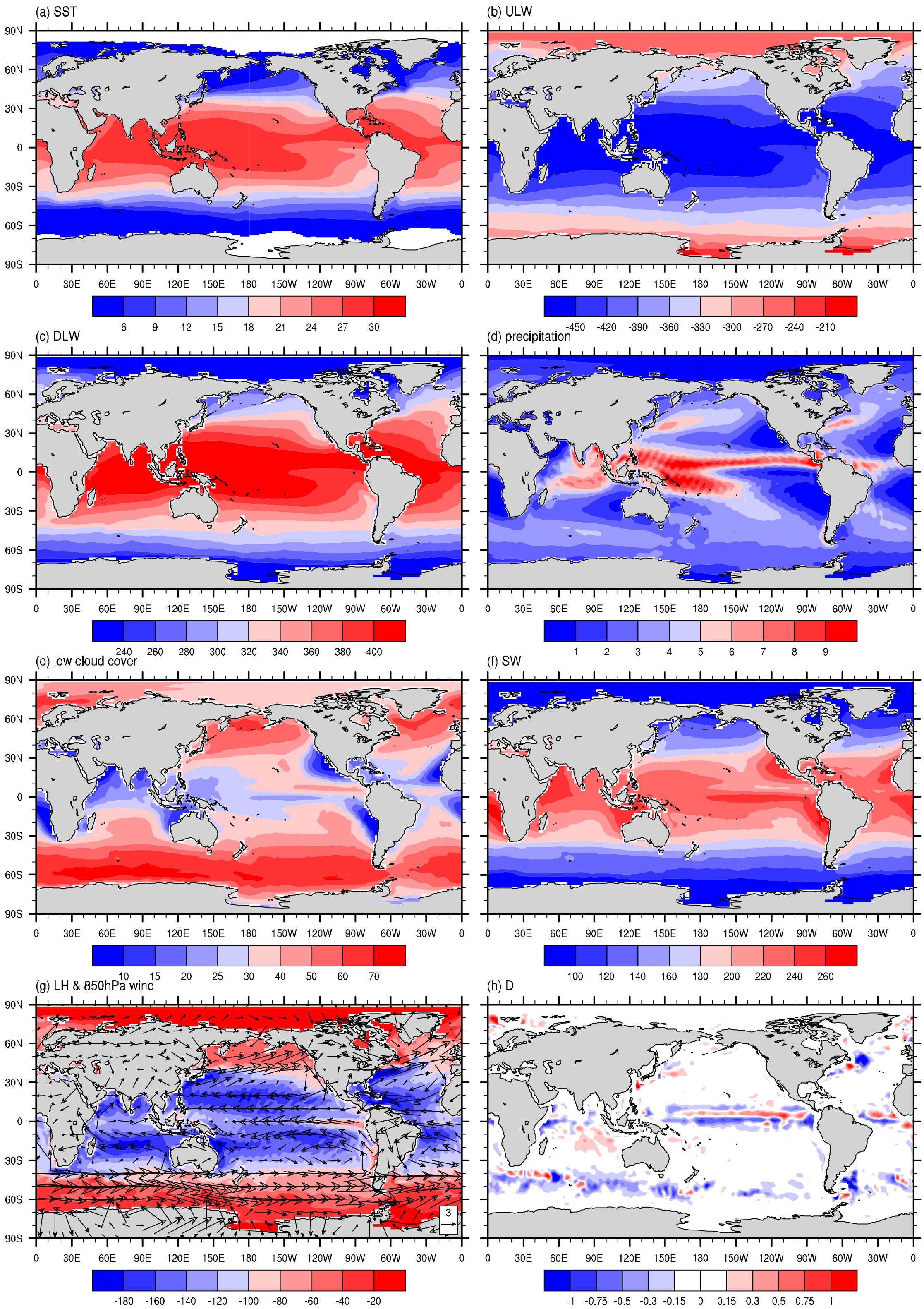

Fig. 4 Horizontal distributions of long-term (1910-2012) mean fields of (a) SST (°C), (b) upward longwave radiation (W/m^2), (c) downward longwave radiation

(W/m^2), (d) precipitation ($kg/m^2/day$), (e) low cloud cover (%), (f) net shortwave radiation (W/m^2), (g) surface latent heat flux (W/m^2) and 850hPa wind (m/s), and (h) the sum of three dimensional ocean advection terms (°C/mon).

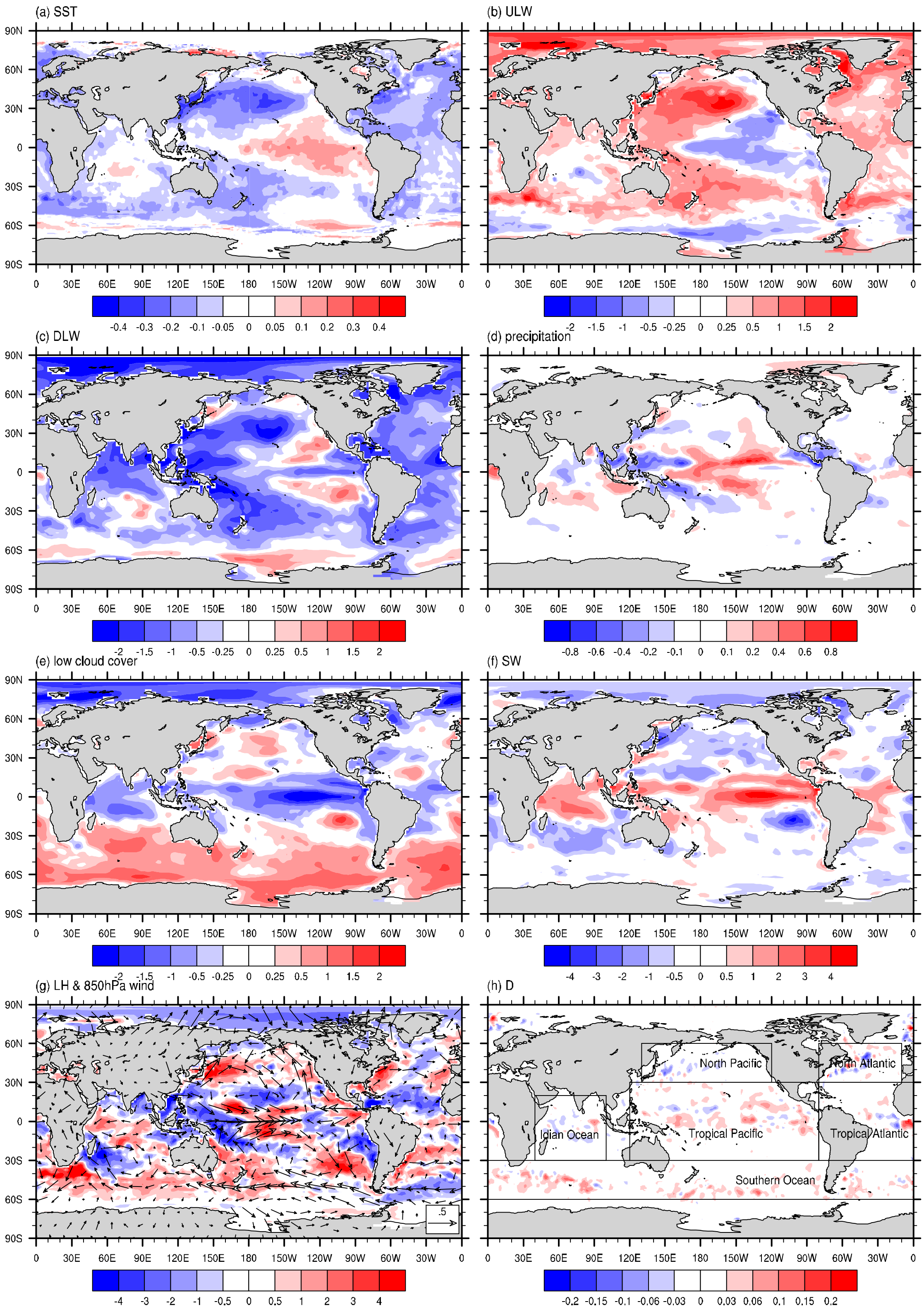

Fig. 5 Same as Fig. 4 except for the difference between the composite warming phases and the long-term mean.

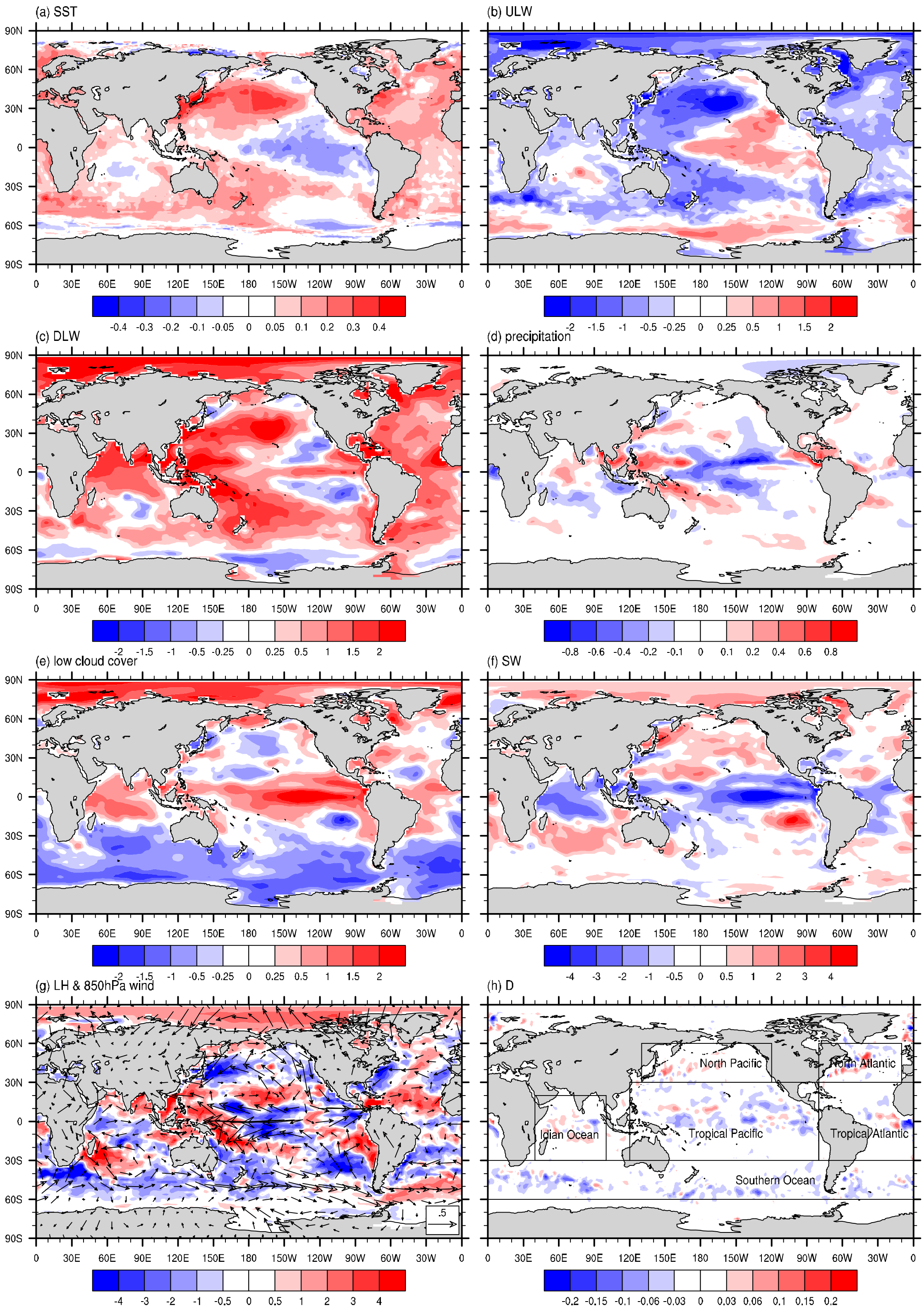

Fig. 6 Same as Fig. 4 except for the difference between the composite cooling phases and the long-term mean.

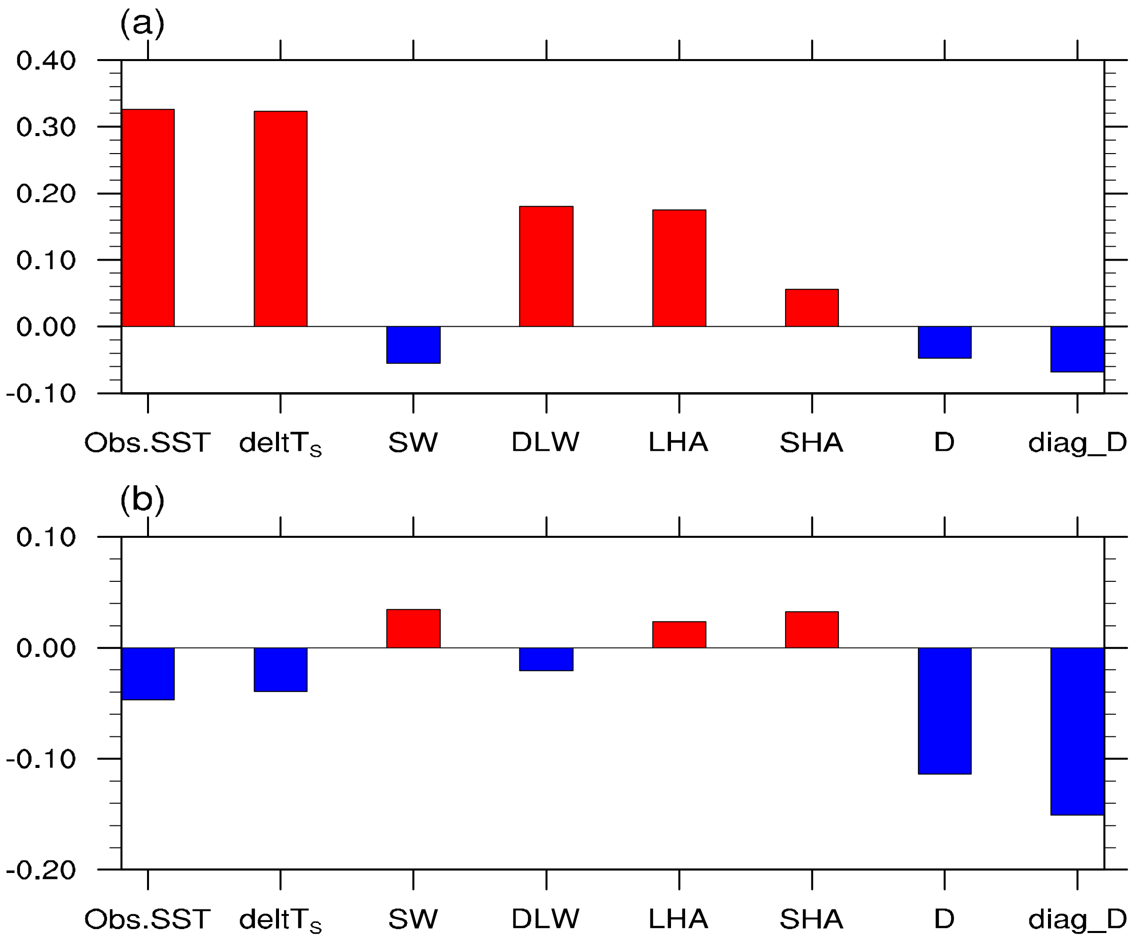

Fig. 7 (a) The observed and diagnosed global mean SST difference (unit: °C.) averaged between E2 and E1 and between E4 and E3 and contributions from each term in the right hand side of equation (3). The first column is the observed SST difference. deltT$_s$ denotes the diagnosed SST difference, which is sum of all terms in the right hand side of equation (3). SW denotes net shortwave radiation, DLW denotes downward longwave radiation, LHA and SHA denote wind induced latent and sensible heat flux terms δQ_{lh}^{a} and δQ_{sh}^{a} , D is the ocean dynamic term derived based on the net heat flux, and diag_D is the ocean dynamic term calculated based on 3D ocean advection. (b) Same as (a) except for the composite average between E3 and E2 and between E5 and E4.

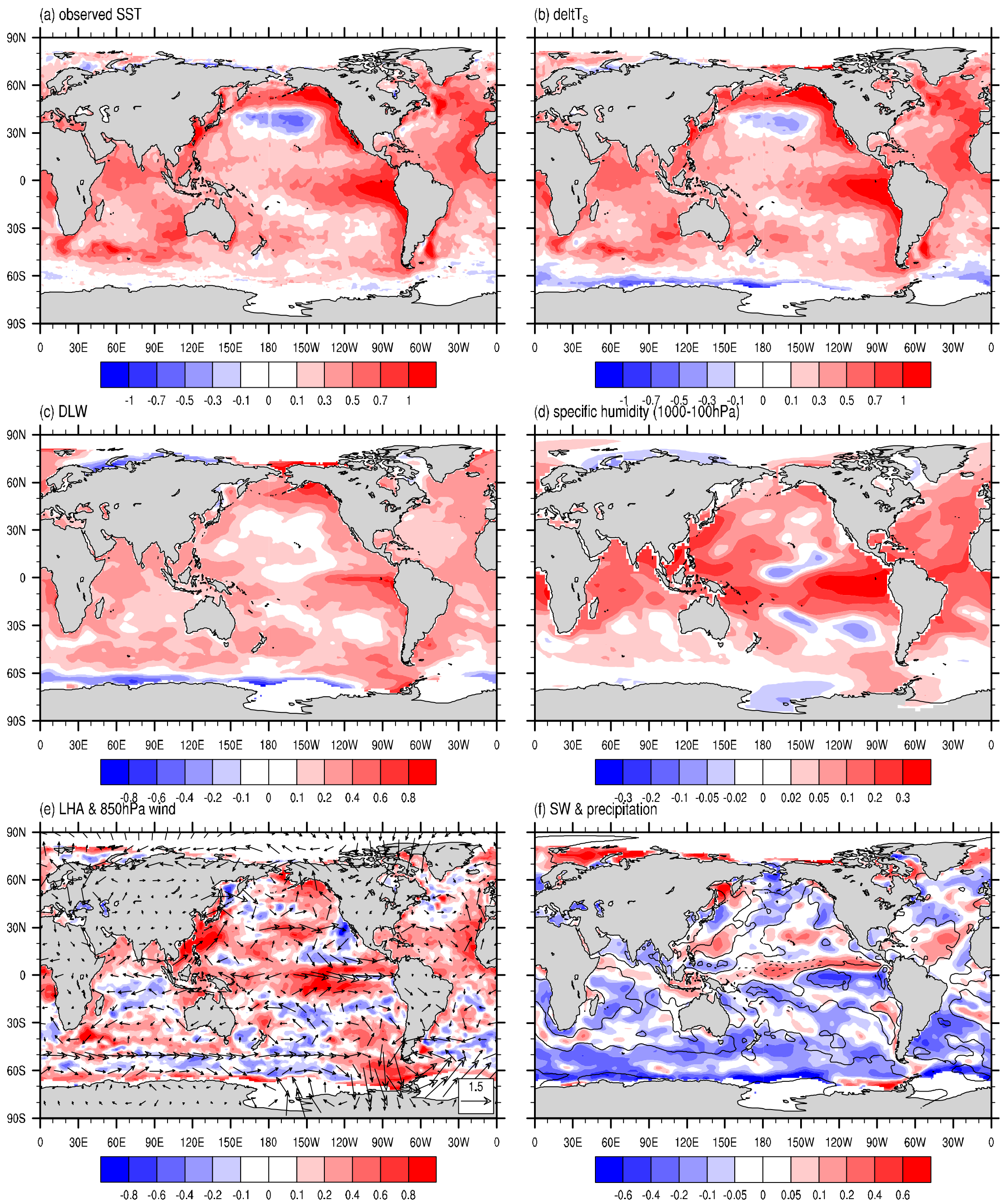

Fig. 8 Horizontal distributions of difference fields averaged between E2 and E1 and between E4 and E3 of (a) observed and (b) diagnosed SST (°C), (c) downward longwave radiation term (°C), (d) column integrated (1000-100hPa) specific humidity (%), (e) wind induced latent heat flux term (°C) and 850hPa wind (m/s), (f) net shortwave radiation term (°C, shaded) and precipitation (kg/m^2/day,

contour, with solid lines representing positive values). All heat flux terms above are calculated based on the right hand side of equation (3) and have a unit of °C.

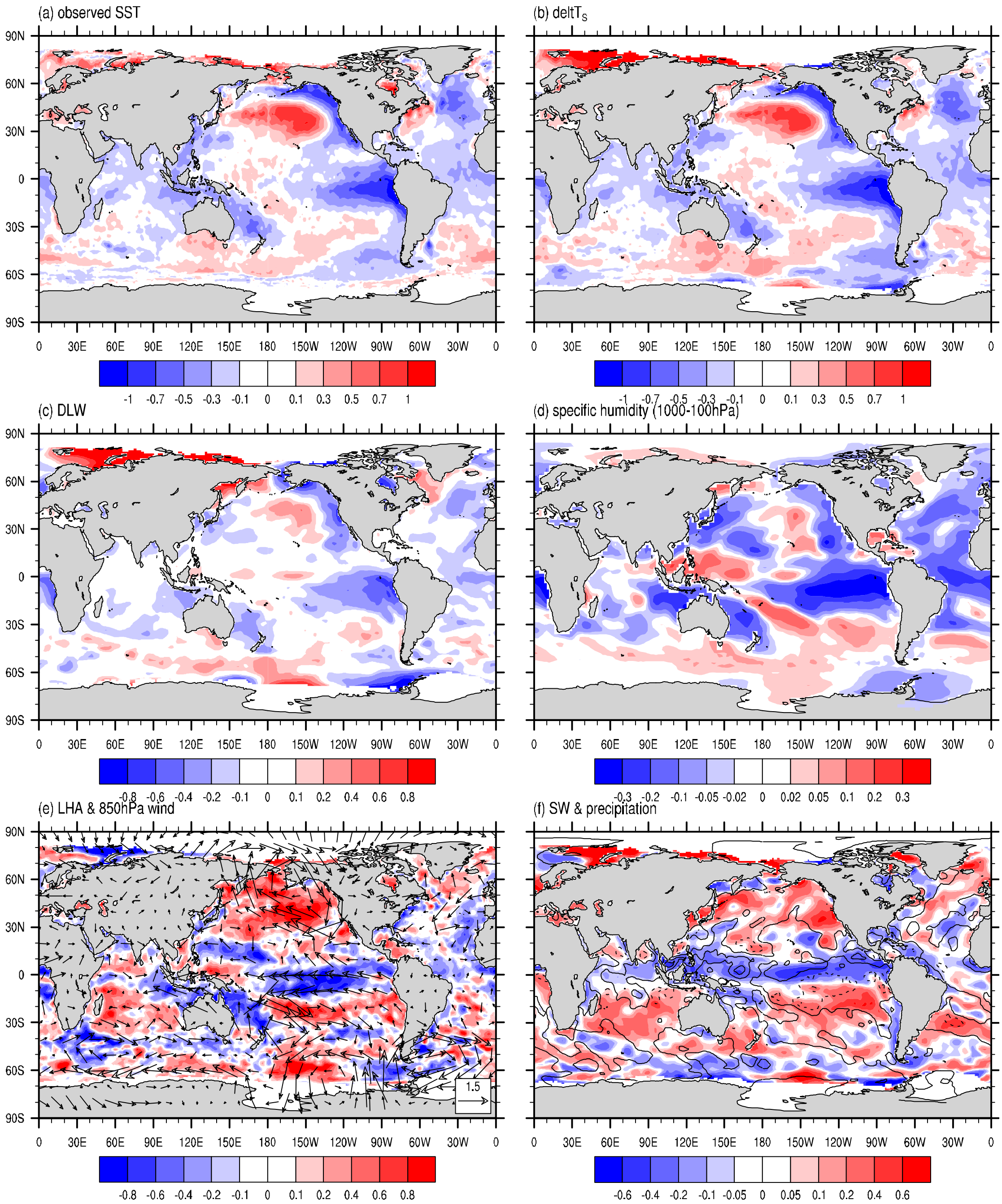

Fig. 9 Same as Fig. 8 except for the composite difference between E3 and E2 and between E5 and E4 during the cooling phases.

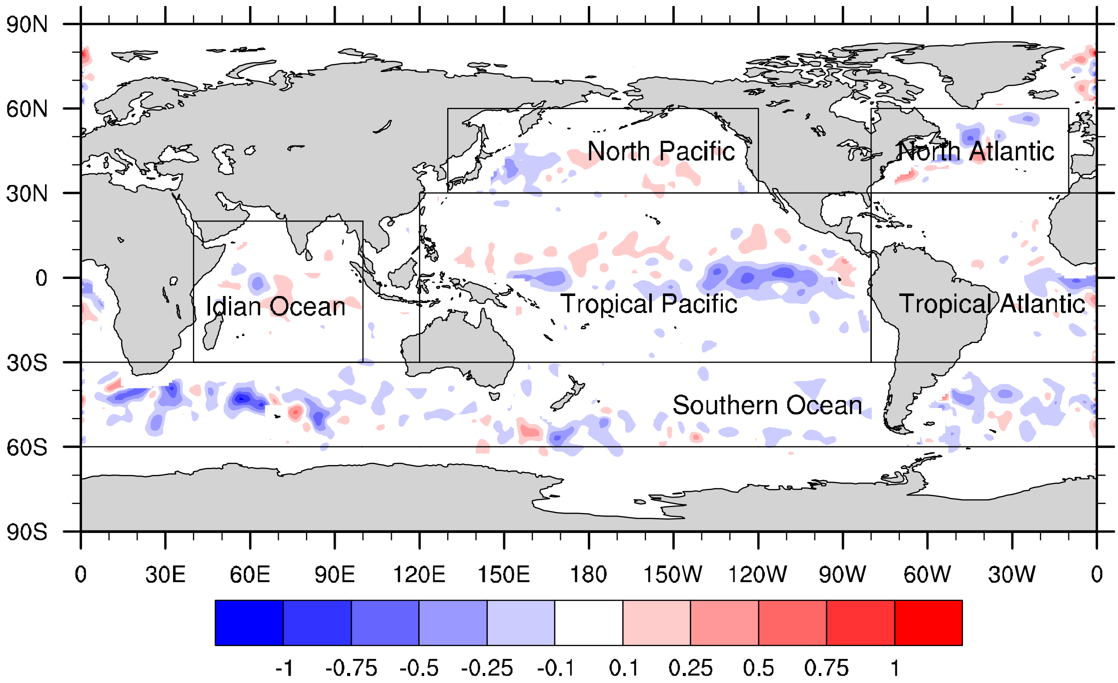

Fig. 10 Same as Fig. 9 except for the difference of the three dimensional ocean advection term (°C).